03 Jul 2023

High-temperature Phonon-assisted Upconversion Photoluminescence Of Monolayer WSe2

Fengkai Meng

Xiaodong Yang
Missouri University of Science and Technology, yangxia@mst.edu

Jie Gao
Missouri University of Science and Technology, gaojie@mst.edu

Recommended Citation

F. Meng et al., "High-temperature Phonon-assisted Upconversion Photoluminescence Of Monolayer WSe2," *Applied Physics Letters*, vol. 123, no. 1, article no. 013502, American Institute of Physics, Jul 2023. The definitive version is available at https://doi.org/10.1063/5.0156364

Applied Physics Letters

RESEARCH ARTICLE | JULY 05 2023

High-temperature phonon-assisted upconversion photoluminescence of monolayer WSe_2

Fengkai Meng ; Xiaodong Yang ; Jie Gao

Appl. Phys. Lett. 123, 013502 (2023)
https://doi.org/10.1063/5.0156364

AIP Publishing

Applied Physics Letters ARTICLE pubs.aip.org/aip/apl

High-temperature phonon-assisted upconversion photoluminescence of monolayer WSe_2

Cite as: Appl. Phys. Lett. **123**, 013502 (2023); doi: 10.1063/5.0156364
Submitted: 28 April 2023 · Accepted: 15 June 2023 ·
Published Online: 5 July 2023

Fengkai Meng,[1] Xiaodong Yang,[2] and Jie Gao[1,a)]

AFFILIATIONS

[1]Department of Mechanical Engineering, Stony Brook University, Stony Brook, New York 11794, USA
[2]Department of Mechanical and Aerospace Engineering, Missouri University of Science and Technology, Rolla, Missouri 65409, USA

[a)]Author to whom correspondence should be addressed: jie.gao.5@stonybrook.edu

ABSTRACT

Phonon-assisted upconversion photoluminescence (UPL) is an anti-Stokes process emitting photons of energy higher than the excitation photons, with upconversion energy gain provided by optical phonons. Atomically thin transition metal dichalcogenides provide a promising platform for exploring the phonon-assisted UPL process due to their strong phonon–exciton interactions. Here, high-temperature phonon-assisted UPL process in monolayer WSe_2 is investigated, aiming to understand the role of phonon population and the number of phonons involved in the UPL process at elevated temperatures. It is demonstrated that the integrated intensity of UPL emission significantly increases by two orders of magnitude as the temperature rises from room temperature of 295 to 476 K, which is distinguished from the photoluminescence emission usually suffering from thermal quenching. The observed growth of UPL emission intensity is attributed to both the increased phonon population and the reduced number of phonons required at elevated temperatures. Our study paves the way toward near-infrared light detection, anti-Stokes energy harvesting, optical refrigeration, and temperature sensing.

Upconversion photoluminescence represents an anti-Stokes process in which the energy of emitting photons is higher than the energy of excitation photons, where the energy gap is compensated by multi-photon absorption,[1] Auger recombination,[2] and phonon absorption.[3,4] The UPL process involves the promotion of electrons excited by low-energy photons at virtual or real intermediate states to high-energy final states, where the real intermediate state can be the defect states, trion states, or electronic subbands.[5] The UPL processes have been observed in various material systems such as quantum dots,[6] quantum wells,[7] carbon nanotubes,[8] rare-earth doped materials,[9] perovskite nanocrystals,[10,11] organic dyes,[12] color centers in diamond,[13] and 2D materials and heterostructures,[14,15] which are useful to realize a variety of applications including bioimaging,[16] optical tweezers,[17] nanoscale thermometry,[13] display,[18] optical refrigeration,[19] and energy harvesting.[20] Specifically, phonon-assisted UPL with upconversion energy gain provided by optical phonons has garnered a lot of interest since it is a one-photon excitation process in linear regime and only requires continuous-wave laser excitation, in contrast to other types of nonlinear upconversion processes.

Monolayer TMDCs with direct bandgaps of 1.0–2.3 eV and strong PL responses in visible and near-infrared frequencies have been extensively studied in the areas of nanoelectronics,[21] photonics,[22] and optoelectronics[23] in recent decades. The strong photon–exciton and phonon–exciton interaction strengths make monolayer TMDCs an intriguing platform for exploring the phonon-assisted UPL process.[24] However, much attention has been paid to the upconversion mechanism[25,26] in monolayer TMDCs at room temperature and low temperatures,[3,27,28] while the investigations on phonon-assisted UPL process at elevated temperatures are still at an early stage. Due to the nature of temperature-dependent phonon behaviors, it will be critical to explore the UPL process at high temperatures and reveal the contribution of phonon occupation to the thermally activated upconversion emission. Unlike PL emission, which typically decreases at high temperatures due to thermal quenching, thermally induced enhancement of UPL emission in monolayer TMDCs is expected, but it has not been explored yet.

In this work, phonon-assisted UPL process in monolayer WSe_2 at high temperatures is demonstrated with temperature-dependent phonon population analysis. The measured UPL emission intensity at high temperatures follows a linear dependence on the excitation power of continuous-wave lasers, which suggests that the UPL is a one-photon involved upconversion process with the energy gain provided by optical phonons. The UPL emission centered at 756 nm with the energy gain of 127 meV is achieved at room temperature under the

excitation of an 820 nm laser. As the temperature increases from 295 to 476 K, the peak wavelength of UPL emission gets redshifted by 89 meV, while the integrated intensity of UPL emission is amplified greatly by 92 folds. The observed temperature-dependent UPL emission is further analyzed by theoretical modeling, revealing the contributions of both the increased phonon population and the reduced number of phonons required in the UPL process as the temperature is increased. The demonstrated results of high-temperature UPL emission in monolayer TMDCs aims to advance promising applications in infrared night vision, upconversion energy harvesting, optical refrigeration, and temperature sensing.

The monolayer WSe_2 is synthesized by molecular-beam epitaxy on sapphire substrate with the size of $\sim$20 μm as shown in the optical microscope image of Fig. 1(a). The measured Raman spectrum of monolayer WSe_2 excited at 633 nm is presented in Fig. 1(a) with two dominant Raman peaks. The peak located at 125 cm^{-1} is attributed to the longitudinal acoustic phonon mode,[14,28] while the peak at 250 cm^{-1} corresponds to the degenerated in-plane E^1_{2g} vibrational phonon mode and out-of-plane A_{1g} phonon mode of Se–W bonds.[29] Figure 1(b) depicts the measured PL and UPL spectra under continuous-wave excitation at the wavelengths of 633, 785, 800, and 820 nm, where short pass filters are used for the UPL emission collection. The dashed lines show the Gaussian–Lorentzian convolution (Voigt) fitting of the UPL spectra. It is observed that UPL emission peak wavelengths are almost unchanged around 756 nm under different excitation wavelengths, which are consistent with the PL emission peak position. The UPL emission peak intensity decreases significantly as the excitation wavelength moves further away from the emission wavelength. The UPL intensity excited at 785 nm is eight times and 61 times stronger than the intensity excited at 800 and 820 nm, respectively, whereas it is 12 times weaker compared to the PL intensity excited at 633 nm. As shown in the inset of Fig. 1(b), the UPL emission peak intensity decays exponentially as a function of the upconversion energy gain $\Delta E = \hbar\omega_{UPL} - \hbar\omega_{exc}$, where $\hbar\omega_{UPL}$ and $\hbar\omega_{exc}$ represent the UPL emission photon energy and the excitation photon energy, respectively. Upconversion energy gains of 57, 96, and 127 meV are obtained at the excitation wavelengths of 785, 800, and 820 nm, respectively. The UPL emission with below-bandgap excitation is mediated by the absorption of multiple A_{1g} phonons ($\sim$31 meV in monolayer WSe_2), which couple to an intermediate state, and then followed by the carrier relaxation to the band edge and the exciton recombination. It is noteworthy that the observed multiphonon-assisted UPL emission is distinguished from the phonon-cascade hot PL emission with above-bandgap excitation where periodic discrete emission peaks in the anti-Stokes spectral range are observed.[30]

To gain more detailed insight into the UPL emission, the PL spectra excited at 633 nm and UPL spectra excited at 820 nm under different excitation powers at room temperature are measured, as illustrated in Figs. 2(a) and 2(b). It is noted that UPL intensity goes up gradually with the increased excitation power, while the spectral profile is maintained. Figure 2(c) further plots the integrated PL and UPL intensity as a function of excitation power in a log –log scale at different excitation wavelengths. The integrated emission intensity is fitted by a power law $I = \alpha P^{\beta}$, where α is the fitting parameter, P is the excitation power, and β is the exponent of the power law. The fitted β values are very close to 1 for all excitation wavelengths, indicating the one-photon involved phonon-assisted UPL emission process in the linear regime, which is distinct from the nonlinear optical phenomenon like two-photon absorption[31] or Auger recombination.[32,33] According to the ratio of the upconversion energy gain and the phonon energy at the excitation wavelengths of 785, 800, and 820 nm, the number of phonons involved in the measured UPL process are estimated from 2 to 4 in monolayer WSe_2.

Furthermore, the effect of elevated temperature on the UPL emission in monolayer WSe_2 is investigated. A Linkam THMS600 heating stage is utilized for the UPL characterization at high temperatures. Figure 3(a) shows the power-dependent UPL spectra at 386 K under the excitation wavelength of 820 nm, where the UPL emission intensity linearly increases with the excitation power and the peak wavelength is redshifted to 781 nm. Figure 3(b) compares the UPL spectra measured at 386 and 296 K excited at 820 nm under the same excitation power of 5.67 mW. A 25 nm redshift of UPL emission peak wavelength and a tenfold increase in UPL emission intensity are observed at 386 K, compared to the case at 296 K. Figure 3(c) further displays the UPL spectra obtained at three elevated temperatures of 316, 386, and 438 K, where longer UPL emission peak wavelength and stronger UPL emission intensity are observed at the higher temperature. Specifically, as the temperature increases from 316 to 438 K, the peak wavelength is shifted from 758 to 789 nm, while the emission intensity is enhanced 17 times. Figure 3(d) plots the integrated UPL intensity as a function of the excitation power at room temperature and three elevated temperatures. The fitted near-unity β values manifest that the observed UPL processes at elevated temperatures are also within the one-photon regime.

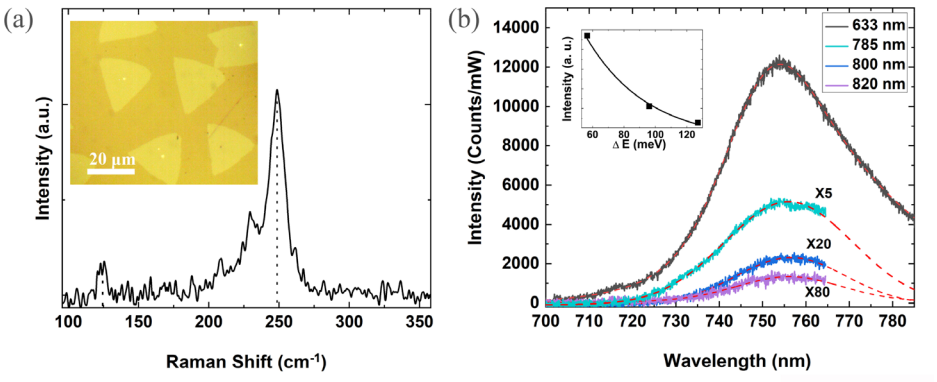

FIG. 1. (a) Raman spectrum and optical image of monolayer WSe_2 on a sapphire substrate. (b) UPL spectra of monolayer WSe_2 at excitation wavelengths of 785 nm (cyan), 800 nm (blue), and 820 nm (magenta), and conventional PL spectrum excited at 633 nm (black). The inset figure shows the UPL intensity with respect to the energy gain ΔE, which follows the exponential decay.

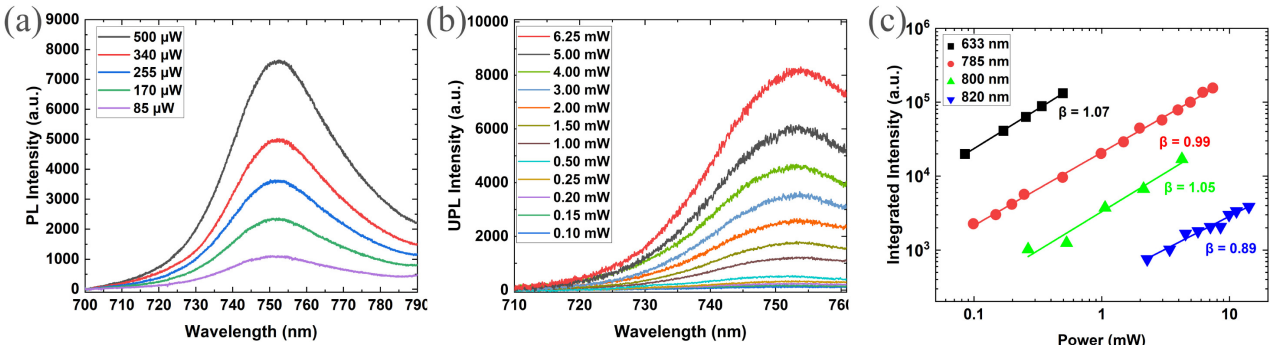

FIG. 2. Measured power-dependent PL and UPL spectra of monolayer WSe_2 at room temperature excited at (a) 633 and (b) 785 nm, respectively. (c) Integrated intensity of PL excited at 633 nm (black square) and UPL excited at 785 nm (red dot), 800 nm (green up-pointing triangle), and 820 nm (blue down-pointing triangle) as a function of the excitation power.

Temperature-dependent UPL emission in monolayer WSe_2 from 295K to 465 K is further analyzed to understand the electron–phonon and phonon–exciton interactions in the UPL process at elevated temperatures. Figures 4(a) and 4(b) depict the temperature-dependent PL and UPL spectra excited at 633 and 820 nm. It is noted that PL emission peak intensity decreases about 5 times, but the UPL emission peak intensity increases significantly by 42 times as the temperature increases from 295 to 465 K. Figures 4(c) and 4(d) plot the PL and UPL emission peak wavelength and integrated intensity extracted from the measured spectra as a function of temperature. As shown in Fig. 4(c), the UPL emission peak wavelength (energy) redshifts gradually from 755 nm (1.64 eV) to 799 nm (1.55 eV) as the temperature increases from 295 to 465 K, while the PL emission peak wavelength also follows a similar trend. The temperature-dependent shift of the PL and UPL peak energy can be fitted by the modified Varshni equation $E_g(T) = E_g(0) - S\langle\hbar\omega_{AC}\rangle\left[\coth\left(\frac{\langle\hbar\omega_{AC}\rangle}{2k_BT}\right) - 1\right]$ that describes the bandgap dependence of temperature, where $E_g(0)$ is the excitonic transition energy at $T = 0$ K, S is a dimensionless constant describing the electron–phonon coupling strength, $\langle\hbar\omega_{AC}\rangle$ represents the average acoustic phonon energy involved in electron–phonon interactions, and k_B is the Boltzmann constant.[34,35] For monolayer WSe_2, $\langle\hbar\omega_{AC}\rangle = 15$ meV, which corresponds to the 125 cm^{-1} peak in the Raman spectrum. The theoretical fittings are presented as the solid

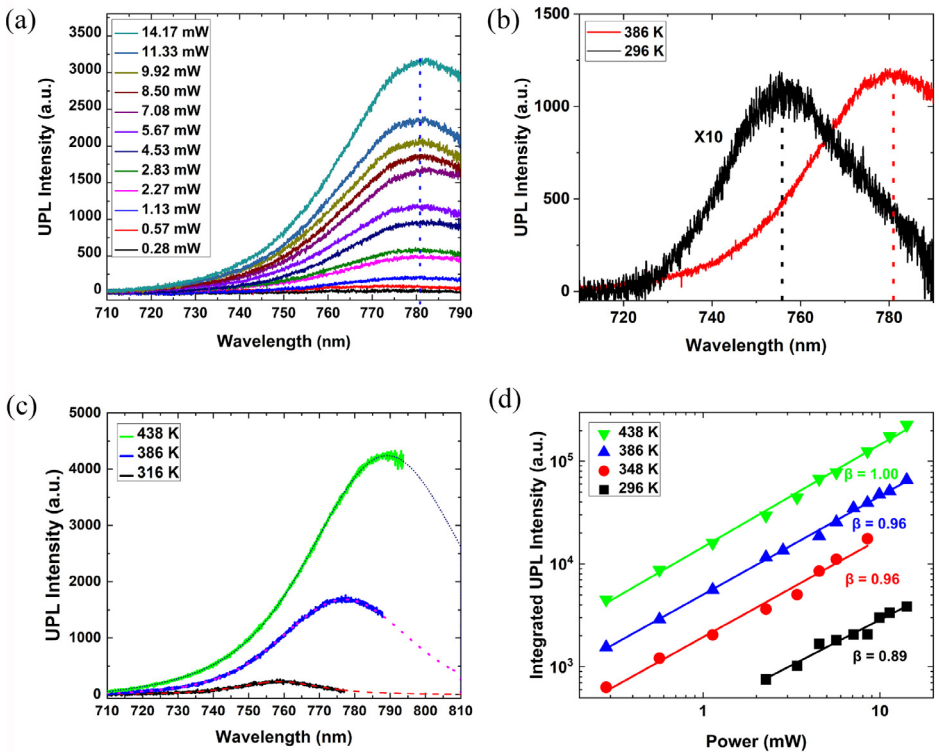

FIG. 3. (a) UPL spectra excited at 820 nm under different excitation powers at the elevated temperature of 386 K. (b) Comparison of UPL spectra measured at 386 K (black) and 296 K (red) excited at 820 nm under the same excitation power. (c) UPL spectra measured at three elevated temperatures of 316, 386, and 438 K excited at 820 nm under the same excitation power. (d) Power-dependent integrated UPL intensity plotted in a log–log scale measured at 296 K (black square), 348 K (red dot), 386 K (blue up-pointing triangle), and 438 K (green down-pointing triangle).

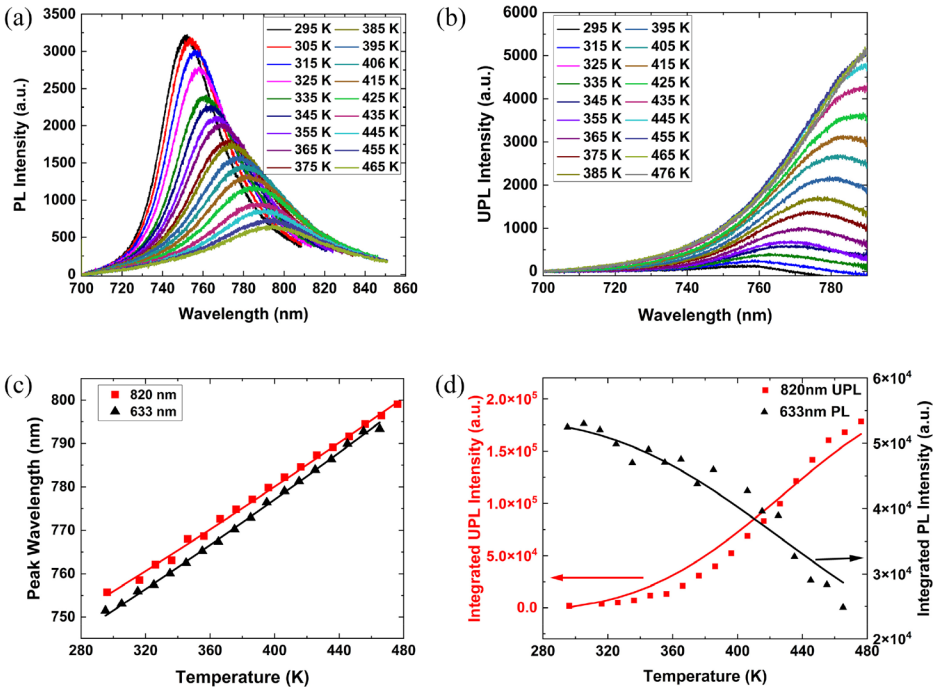

FIG. 4. Temperature-dependent (a) PL spectra excited at 633 nm and (b) UPL spectra excited at 820 nm. (c) PL and UPL emission peak wavelength as a function of temperature. (d) PL and UPL integrated emission intensity as a function of temperature. Measured data are shown as red squares and black triangles, and the theoretical fittings are represented by solid lines.

lines in Fig. 4(c) with $E_g(0) = 1.753$ eV and $S = 2.95$ for the UPL process, while $E_g(0) = 1.772$ eV and $S = 3.19$ for the PL process. It is found that the measured temperature-dependent PL and UPL peak energy follows the Varshni equation well. The slightly different S and $E_g(0)$ values between the PL and UPL processes indicate the distinguished electron–phonon and phonon–exciton interactions existing in the temperature-dependent PL and UPL emission processes in monolayer WSe_2. As illustrated in Fig. 4(d), the integrated intensity of PL emission decreases gradually with temperature due to the thermal quenching of excitons, which follows the Arrhenius equation $I_{PL}(T) = I_0/[1 + R\exp(-E_a/k_BT)]$, where I_0 is the PL intensity at $T = 0$ K, E_a is the thermal activation energy that dissociates the excitons, R represents the ratio between the nonradiative and radiative recombination rates.[36,37] The experimental results for the PL process in monolayer WSe_2 are well fitted by the black solid line with $R = 300$ and $E_a = 234$ meV. On the contrary, distinguished from the PL process, the integrated intensity of UPL emission significantly increases by 92 folds as the temperature rises from room temperature of 295 to 476 K, due to the enhanced phonon population available in monolayer WSe_2 at high temperatures. The evolution of UPL emission with temperature increase can be revealed by the phonon population of transverse optical phonons $N(T) = [\exp(\hbar\omega_{TO}/k_BT) - 1]^{-1}$. The integrated intensity of multiphonon-assisted UPL emission is proportional to the nth power of the phonon population described as $I_{UPL}(T) \propto N^n(T)$, where $n = \Delta E/\hbar\omega_{TO}$ is the effective number of phonons involved in the UPL process, $\Delta E(T) = \hbar\omega_{UPL}(T) - \hbar\omega_{exc}$ is the upconversion energy gain, and $\hbar\omega_{TO} = 31$ meV is the transverse optical phonon energy in monolayer WSe_2, which corresponds to the 250 cm^{-1} Raman peak. The observed growth of UPL emission intensity is attributed to both the increased phonon population $N(T)$ and the reduced number of phonons n at the elevated temperatures. The increased phonon population $N(T)$ of the transverse optical phonons at high temperatures leads to strong phonon–exciton interactions in monolayer WSe_2, which enhances the phonon-mediated UPL photon emission. At the same time, the decreased energy gain $\Delta E(T)$ at high temperatures results in the reduced number of phonons participating in the upconversion anti-Stokes process from $n \approx 4$ to 1, which will further amplify the multiphonon-assisted UPL emission. As displayed in Fig. 4(d), the measured data agree well with the theoretical modeling shown as the red solid line, manifesting the advantage of utilizing temperature-controlled phonon population to benefit the phonon-mediated UPL process.

In summary, high-temperature multiphonon-assisted UPL of monolayer WSe_2 has been demonstrated with the upconversion energy gain between emission photon energy and excitation photon energy compensated by optical phonons. At elevated temperatures, the linear dependence of UPL intensity on the excitation power indicates the one-photon upconversion process. It is observed that when temperature increases from 295 to 476 K, the peak wavelength of UPL emission has a redshift of 89 meV due to electron-phonon interactions, resulting in the reduction of number of phonons required for the UPL process. Meanwhile, the integrated intensity of UPL emission grows significantly by two orders of magnitude due to the phonon-exciton interactions, which is strengthened by the increased phonon population and the reduced number of phonons required in the UPL process at high temperatures. These results demonstrate that temperature provides an effective tuning mechanism for manipulating the UPL emission wavelength and intensity in TMDC monolayers, which will further benefit the applications of thermally tunable TMDC photonics, infrared night vision, upconversion energy harvesting, optical refrigeration, and temperature sensing. In addition to the high

temperature effect on the enhanced UPL emission, it is worth noting that other effects such as doping, encapsulation, and substrate on UPL emission in TMDCs are exciting to be explored in the future.

The authors acknowledge the support from the DARPA (No. W911NF2110353).

AUTHOR DECLARATIONS

Conflict of Interest

The authors have no conflicts to disclose.

Author Contributions

Fengkai Meng: Formal analysis (lead); Writing – original draft (lead). **Xiaodong Yang:** Conceptualization (equal); Investigation (equal); Writing – review & editing (equal). **Jie Gao:** Conceptualization (lead); Investigation (equal); Writing – review & editing (lead).

DATA AVAILABILITY

The data that support the findings of this study are available from the corresponding author upon reasonable request.

REFERENCES

[1]M. Wu, D. N. Congreve, M. W. B. Wilson, J. Jean, N. Geva, M. Welborn, T. Van Voorhis, V. Bulovic, M. G. Bawendi, and M. A. Baldo, Nat. Photonics **10**, 31 (2016).
[2]H. M. Cheong, B. Fluegel, M. C. Hanna, and A. Mascarenhas, Phys. Rev. B **58**, R4254 (1998).
[3]J. Jadczak, L. Bryja, J. Kutrowska-Girzycka, P. Kapuściński, M. Bieniek, Y.-S. Huang, and P. Hawrylak, Nat. Commun. **10**, 107 (2019).
[4]A. M. Jones, H. Yu, J. R. Schaibley, J. Yan, D. G. Mandrus, T. Taniguchi, K. Watanabe, H. Dery, W. Yao, and X. Xu, Nat. Phys. **12**, 323 (2016).
[5]Q. Wang and A. T. S. Wee, J. Phys.: Condens. Matter. **33**, 223001 (2021).
[6]W. Zhou, Y. Shang, F. P. G. de Arquer, K. Xu, R. Wang, S. Luo, X. Xiao, X. Zhou, R. Huang, E. Sargent, and Z. Ning, Nat. Electron. **3**, 251 (2020).
[7]G. Bacher, C. Hartmann, H. Schweizer, T. Held, G. Mahler, and H. Nickel, Phys. Rev. B **47**, 9545 (1993).
[8]N. Akizuki, S. Aota, S. Mouri, K. Matsuda, and Y. Miyauchi, Nat. Commun. **6**, 8920 (2015).
[9]F. Auzel, Chem. Rev. **104**, 139–174 (2004).
[10]A. G. del Aguila, T. T. H. Do, J. Xing, W. J. Jee, J. B. Khurgin, and Q. Xiong, Nano Res. **13**, 1962 (2020).
[11]W. Zhang, Y. Ye, C. Liu, J. Wang, J. Ruan, X. Zhao, and J. Han, Adv. Opt. Mater. **9**, 2001885 (2021).
[12]W. Zou, C. Visser, J. A. Maduro, M. S. Pshenichnikov, and J. C. Hummelen, Nat. Photonics **6**, 560 (2012).
[13]T. T. Tran, B. Regan, E. A. Ekimov, Z. Mu, Y. Zhou, W. Gao, P. Narang, A. S. Solntsev, M. Toth, I. Aharonovich, and C. Bradac, Sci. Adv. **5**, eaav9180 (2019).
[14]Z. Chu, A. Han, C. Lei, S. Lopatin, P. Li, D. Wannlund, D. Wu, K. Herrera, X. Zhang, A. H. MacDonald, X. Li, L.-J. Li, and K. Lai, Nano Lett. **18**, 7200 (2018).
[15]E. Zuberek, M. Majak, J. Lubczynski, J. Debus, K. Watanabe, T. Taniguchi, C. H. Ho, L. Bryja, and J. Jadczak, Sci. Rep. **12**, 13699 (2022).
[16]F. Wang, R. Deng, J. Wang, Q. Wang, Y. Han, H. Zhu, X. Chen, and X. Liu, Nat. Mater. **10**, 968 (2011).
[17]X. Shan, F. Wang, D. Wang, S. Wen, C. Chen, X. Di, P. Nie, J. Liao, Y. Liu, L. Ding, P. J. Reece, and D. Jin, Nat. Nanotechnol. **16**, 531 (2021).
[18]R. Deng, F. Qin, R. Chen, W. Huang, M. Hong, and X. Liu, Nat. Nanotechnol. **10**, 237 (2015).
[19]S.-T. Ha, C. Shen, J. Zhang, and Q. Xiong, Nat. Photonics **10**, 115 (2016).
[20]J. Wu, Z. Yang, C. Qiu, Y. Zhang, Z. Wu, J. Yang, Y. Lu, J. Li, D. Yang, R. Hao, E. Li, G. Yu, and S. Lin, Nanoscale **10**, 8023 (2018).
[21]D. Akinwande, N. Petrone, and J. Hone, Nat. Commun. **5**, 5678 (2014).
[22]L. Yuan, B. Zheng, J. Kunstmann, T. Brumme, A. B. Kuc, C. Ma, S. Deng, D. Blach, A. Pan, and L. Huang, Nat. Mater. **19**, 617 (2020).
[23]Q. Wang, Q. Zhang, X. Luo, J. Wang, R. Zhu, Q. Liang, L. Zhang, J. Z. Yong, C. P. Y. Wong, G. Eda, J. H. Smet, and A. T. S. Wee, ACS Appl. Mater. Interfaces **12**, 45235 (2020).
[24]B. R. Carvalho, L. M. Malard, J. M. Alves, C. Fantini, and M. A. Pimenta, Phys. Rev. Lett. **116**, 089904 (2016).
[25]H. Li, Y. Ma, Y. Sui, Y. Tang, K. Wei, X. Cheng, and T. Jiang, Nanophotonics **9**, 4809 (2020).
[26]J. Jadczak, M. Glazov, J. Kutrowska-Girzycka, J. J. Schindler, J. Debus, C. H. Ho, K. Watanabe, T. Taniguchi, M. Bayer, and L. Bryja, ACS. Nano **15**, 19165 (2021).
[27]J. Huang, T. B. Hoang, and M. H. Mikkelsen, Sci. Rep. **6**, 22414 (2016).
[28]A. Mushtaq, X. Yang, and J. Gao, Opt. Express **30**, 45212 (2022).
[29]P. Tonndorf, R. Schmidt, P. Böttger, X. Zhang, J. Börner, A. Liebig, M. Albrecht, C. Kloc, O. Gordan, D. R. T. Zahn, S. M. de Vasconcellos, and R. Bratschitsch, Opt. Express **21**, 4908 (2013).
[30]I. Paradisanos, G. Wang, E. M. Alexeev, A. R. Cadore, X. Marie, A. C. Ferrari, M. M. Glazov, and B. Urbaszek, Nat. Commun. **12**, 538 (2021).
[31]N. Dong, Y. Li, S. Zhang, N. McEyoy, R. Gatensby, G. S. Duesberg, and J. Wang, ACS. Photonics **5**, 1558 (2018).
[32]B. Han, C. Robert, E. Courtade, M. Manca, S. Shree, T. Amand, P. Renucci, T. Taniguchi, K. Watanabe, X. Marie, L. E. Golub, M. M. Glazov, and B. Urbaszek, Phys. Rev. X **8**, 031073 (2018).
[33]M. Manca, M. M. Glazov, C. Robert, F. Cadiz, T. Taniguchi, K. Watanabe, E. Courtade, T. Amand, P. Renucci, X. Marie, G. Wang, and B. Urbaszek, Nat. Commun. **8**, 14927 (2017).
[34]K. P. O'donnell and X. Chen, Appl. Phys. Lett. **58**, 2924 (1991).
[35]S. Tongay, J. Zhou, C. Ataca, K. Lo, T. S. Matthews, J. Li, J. C. Grossman, and J. Wu, Nano Lett. **12**, 5576 (2012).
[36]J. D. Lambkin, D. J. Dunstan, K. P. Homewood, L. K. Howard, and M. T. Emeny, Appl. Phys. Lett. **57**, 1986 (1990).
[37]M. Leroux, N. Grandjean, B. Beaumont, G. Nataf, F. Semond, J. Massies, and P. Gibart, J. Appl. Phys. **86**, 3721 (1999).